Available online at www.sciencedirect.com

SciVerse ScienceDirect

Procedia Engineering 27 (2012) 616 – 624

Procedia Engineering

www.elsevier.com/locate/procedia

2011 Chinese Materials Conference

Sillenite-type bismuth ferric nanocrystals: microwave hydrothermal synthesis, structural characterization, and visible-light photocatalytic properties

Qiming Hang[a], Xinhua Zhu[a,*], Jianmin Zhu[a], and Zhiguo Liu[b]

[a]*National Laboratory of Solid State Microstructures, School of Physics, Nanjing University, Nanjing 210093, China*
[b]*National Laboratory of Solid State Microstructures, Department of Materials Science and Engineering, Nanjing University, Nanjing 210093, China*

Abstract

In this work, we report on an efficient visible-light-responsive novel photocatalyst based on sillenite-type bismuth ferric nanocrystals with hexagonal-shaped morphology and particle size range of 18 - 33 nm, which were synthesized by microwave hydrothermal method. Their microstructures were characterized by X-ray diffraction, Raman spectra, X-ray photoelectron spectroscopy and transmission electron microscopy. The high photocatalytic activity was evaluated by degrading the rhodamine B in aqueous solution under visible-light irradiation. The present results demonstrate that the sillenite-type bismuth ferritic nanocrystals are promising visible-light-responsive photocatalysts for degradation of organic compounds.

Keywords: sillenite-type bismuth ferric nanocrystals; microwave hydrothermal synthesis; microstructural characterization; photocatalytic activity

1. Introduction

Recently the research of photocatalysis has become attractive due to the increasingly serious environmental problems. As one of the efficient semiconductor photocatalysts, TiO_2 nanoparticles have been extensively investigated due to their excellent photochemical stability, low cost, and non-toxicity [1-3]. However, the photo-efficiency of TiO_2-based photocatalyst is severely limited by its large band gap (3.2 eV) and the associated restriction of the absorption in the visible-light region, which renders the

*Corresponding author. Tel.: +86-25-83592772; fax: +86-25-83595535.
E-mail address: xhzhu@nju.edu.cn (X.H. Zhu).

 doi:10.1016/j.proeng.2011.12.496

overall process impractical. Therefore, the development of a new material that can be used for the degradation of organic compounds under visible-light irradiation is becoming more and more attractive. Recently, sillenite-type compounds belonging to the polar cubic group (*I*23) with a general formula $Bi_{12}MO_{20}$ (M = Fe, Pb, Ni, Al) that are widely applied in the fields of electrooptics, acoustics, peizotechnics and electronics [4], have been exploited as novel photocatalysts. With the band-gap about 2.2 ~ 3.2 eV the sillenite-type compounds possess higher visible-light-responsive abilities than the TiO_2-based photocatalyst [5,6]. Up to date, several novel photocatalysts such as $Bi_{12}TiO_{20}$, $Bi_{24}Al_2O_{39}$, $Bi_{12}GeO_{20}$, $Bi_{24}GaO_{39}$, $Bi_{12}PbO_{19}$ and $Bi_{12}NiO_{19}$ were reported [6,7]. The most exciting feature is that the photocatalytic activities of these materials are high enough to be comparable to that of TiO_2 under UV-light irradiation. However, the photocatalytic activities of the sillenite-type bismuth ferric nanocrystals still remain unknown although micrometer-sized tetrahedral or triangular pyramidal sillenite-type bismuth ferric crystals were synthesized by hydrothermal process [8].

In this work, we report on an efficient novel visible-light-responsive photocatalyst based on sillenite-type bismuth ferric nanocrystals with composition of $Bi_{12}Fe_{0.63}O_{18.945}$. Such single crystalline sillenite-type nanocrystals with hexagonal-shaped morphology and particle size range of 18 - 33 nm were synthesized *via* microwave hydrothermal process at low temperatures. Their phase structures and morphologies were characterized by a number of instrumental analysis techniques, and the visible-light photocatalytic activities were also evaluated by the degradation of rhodamine B (Rh B, $C_{28}H_{31}ClN_2O_3$) in aqueous solution under visible-light irradiation.

2. Experimental procedure

The sillenite-type bismuth ferric nanocrystals were synthesized *via* microwave hydrothermal process using an equal molar ratio mixture of $Bi(NO_3)_3{\cdot}5H_2O$ and $Fe(NO_3)_3{\cdot}9H_2O$, while KOH solution was used as the mineralizer. First, 0.002 mol $Bi(NO_3)_3{\cdot}5H_2O$ and 0.002 mol $Fe(NO_3)_3{\cdot}9H_2O$ was dissolved separately in double-distilled water, and HNO_3 was added to dissolve the Bi precursors completely. The Fe solution was added to the Bi solution, forming a colorless solution. In a separate beaker, an aqueous KOH solution (8 *M*) was prepared. The Bi-Fe mixed solution was dropped into the clear solution of KOH under magnetic stirring, and then the mixture was transferred into a Telfon reactor (CEM, XP1500) and placed in a microwave oven (MARS-5, CEM). The microwave reaction was carried out at 180°C for 60 minutes, and then cooled to room temperature naturally. The final products were collected by centrifugation, rinsed with distilled water, and dried at 70 °C for 8 hours before further characterization.

Phase structures and morphologies of the sillenite-type bismuth ferric nanocrystals were characterized by X-ray diffraction (XRD, Philips X'Pert MRD four-circle diffractometer) using Cu $K\alpha$ radiation (λ = 1.54 Å), transmission electron microscopy (TEM, Philips CM20) and high resolution transmission electron microscopy (HRTEM, JEM-4000EX, JEOL). The TEM, HRTEM images and SAED patterns were recorded by Gatan multiscan charge-coupled device (CCD) camera system (Gatan, Model 794). The specimens for TEM and HRTEM examinations were prepared by dispersing the products in ethanol, mixing it in an ultrasonic generator, and putting droplets of this dispersion onto a 300 mesh Cu grid coated with a lacey carbon film. Local crystal structures of the sillenite-type bismuth ferric nanocrystals were further examined by Raman spectroscopy (Jobin Yvon HR800, JY Ltd., Horiba, France) at room-temperature with visible laser light (wavelength 514.5 nm) as the excitation source. The slits were adjusted so that the resolution was 1 cm^{-1}. The valences of Bi, Fe, and O ions in the sillenite-type bismuth ferric nanocrystals were determined by X-ray photoelectron spectroscopy (XPS, ESCALab MK-II). The spectrometer was equipped with a hemi-spherical analyzer and all XPS data presented here were acquired using Mg $K\alpha$ as the X-ray source (1253.6 eV). All binding energies of various peaks were calibrated using the binding energy of C 1s (285.1 eV).

The visible-light photocatalytic behavior of the sillenite-type bismuth ferric nanocrystals was evaluated by degradation of rhodamine B (Rh B, $C_{28}H_{31}ClN_2O_3$) in aqueous solution under visible-light irradiation using a 300 W Xe lamp with a cutoff filter ($\lambda \geq 420$ nm) and at the natural pH value. The initial concentration of RhB was 10 mg/L, and in a typical experiment, 100 mL of Rh B solution was continuously stirred and 0.1g of the as-prepared sillenite-type bismuth ferric nanocrystals was loaded into the Rh B solution (in dark and waiting for 60 min) to ensure the adsorption/desorption equilibrium, and then the solution was irradiation under visible-light. In order to monitor the Rh B concentration in the solution, 3 mL of the solution was taken from the photoreactor at appropriate time intervals. The change in the concentration of the Rh B solution was determined after measuring the intensity of absorption peak of Rh B at 553 nm using a spectrophotometer, from which the percentage of degradation was determined.

3. Results and discussion

Figure 1 shows the XRD pattern of the as-prepared sillenite-type bismuth ferric nanocrystals. It is observed that all the diffraction peaks can be indexed based on a sillenite-type compound $Bi_{12}Fe_{0.63}O_{18.945}$ with a space group of cubic *I*23 and lattice parameter of a = 10.129 Å [8]. And also the impurity phases were not detected, indicating that well-crystallized single phase of sillenite-type compound $Bi_{12}Fe_{0.63}O_{18.945}$ was synthesized in this work. Previously, most sillenite-type crystals were reported to be

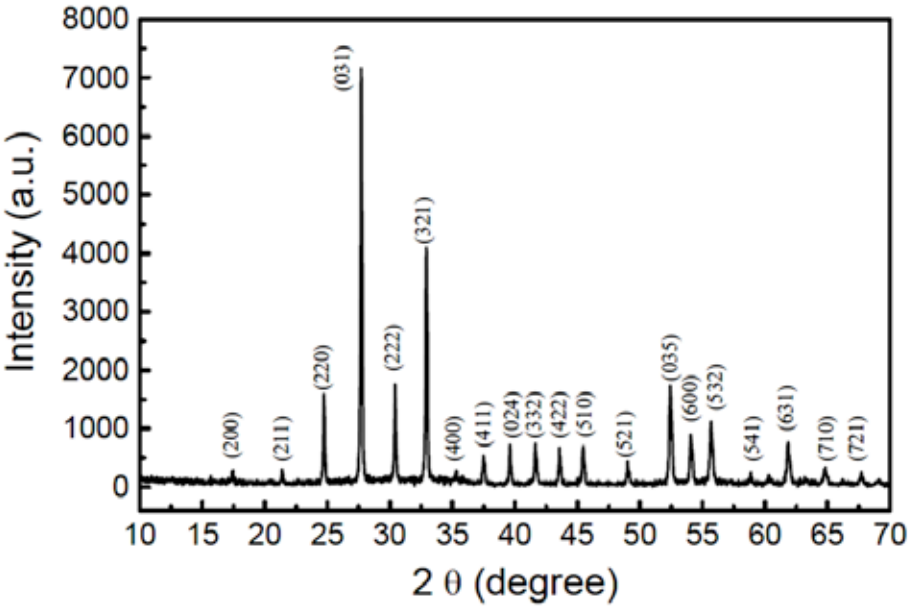

Fig.1. XRD pattern of the as-synthesized sillenite-type bismuth ferric nanocrystals.

grown *via* standard Czochralski method or liquid-phase epitaxy [9,10], however, the synthesis of a sillenite-type compound of $Bi_{12}Fe_{0.63}O_{18.945}$ nanocrystals *via* microwave hydrothermal process, is not reported so far. From the XRD pattern it is also noticed that the forbidden diffraction indexes of the sillenite-type compound $Bi_{12}Fe_{0.63}O_{18.945}$, follow with a rule that the sum of diffraction indexes (*h,k,l*) is odd number, indicating the $Bi_{12}Fe_{0.63}O_{18.945}$ nanocrystals are crystallized in the sillenite body-centered

cubic *I*23 phase.

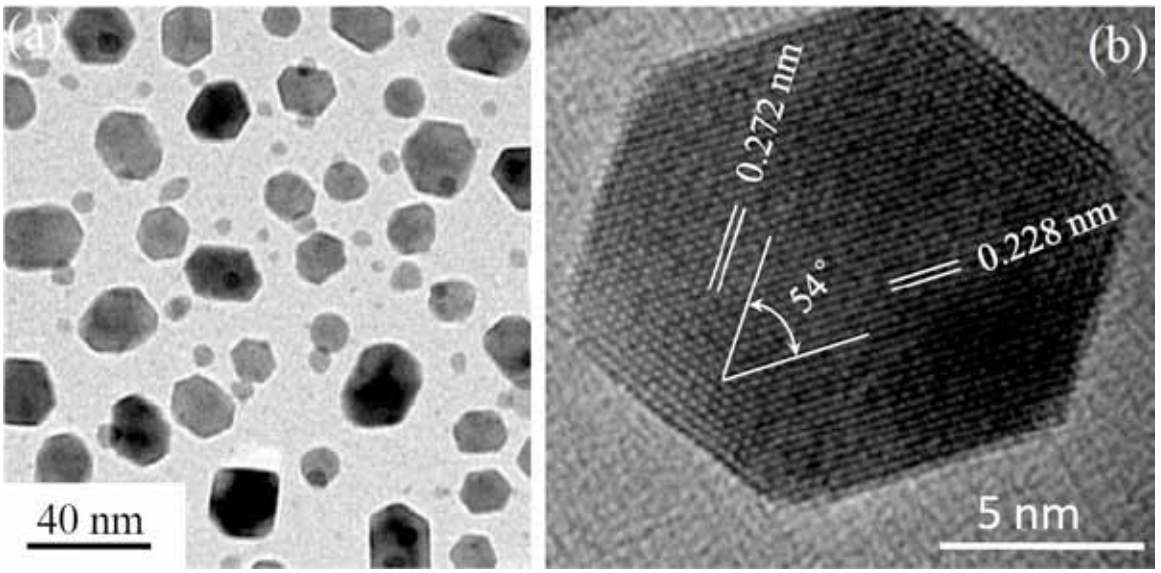

Fig.2.(a) TEM and (b) HRTEM images of the as-synthesized sillenite-type bismuth ferric nanocrystals.

To investigate the particle size and morphology of the as-obtained products, TEM examinations were carried out. Figure 2(a) shows a typical TEM image of the as-prepared sillenite-type bismuth ferric nanocrystals. The product was consisted of nearly hexagonal-shaped crystalline particles with size range from 18 nm to 33 nm. No agglomerated nanocrystals were found, and well dispersive behavior was observed in these sillenite-type $Bi_{12}Fe_{0.63}O_{18.945}$ nanocrystals. In addition, they were also found to be single crystalline, as proven by lattice images of individual particles. A typical lattice image of a single sillenite-type $Bi_{12}Fe_{0.63}O_{18.945}$ particle with hexagonal-shape morphology and a diameter of 13 nm, is shown in Fig. 2(b), in which the lattice fringes are seen to be about 0.272 nm and 0.228 nm, which correspond to the interplanar spacings of the (213) and (420) planes in the sillenite-type $Bi_{12}Fe_{0.63}O_{18.945}$ compound [8]. The angle between the (213) and (420) crystal planes measured from Fig. 2(b) is 54^o, which is very close to the theoretical value of 53.3^o (the angle $\angle$(213):(420) = 53.3^o for $Bi_{12}Fe_{0.63}O_{18.945}$). Therefore, the single-crystalline nature of sillenite-type $Bi_{12}Fe_{0.63}O_{18.945}$ nanocrystals is confirmed by the HRTEM image.

To obtain the information on the local crystal structure of the sillenite-type $Bi_{12}Fe_{0.63}O_{18.945}$ compound from vibrational spectra, Raman scattering investigation was also performed in this work. Figure 3 illustrates the Raman spectrum of the as-produced nanocrystals. Seven major Raman bands centered near 100, 125, 166, 178, 300, 350, and 567 cm^{-1}, were clearly observed. To interpret the observed Raman bands it is necessary to consider the possible numbers of zone-center optical photons in the sillenite

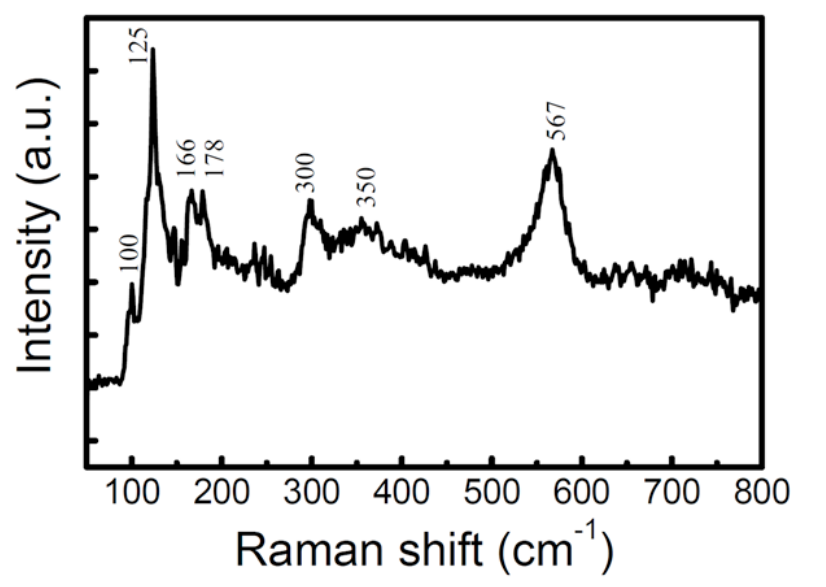

Fig.3. Raman spectrum of the as-synthesized sillenite-type bismuth ferric nanocrystals.

structure. The group-theory analysis predicts that in the sillenite structure with two formula units in the body-centered cell, there are 8*A* (totally symmetric), 8*E* (doubly degenerate), and 24*F* (triply degenerate) zone-center optical phonons, all of them being Raman active and only those of *F* symmetry are IR active [11]. In addition, long-range polarization fields are expected to split the *F* modes into longitudinal-optic (LO) and transverse-optic (TO) phonons, with the former at a higher frequency. In the sillenite-type bismuth ferric nanocrystals with a composition of $Bi_{12}Fe_{0.63}O_{18.945}$, there exists a remarkable deviation from the ideal stoichiometric composition of the sillenite-type compounds, $Bi_{12}MO_{20}$. Fe ions are located in the regular FeO_4 tetrahedra, while 37% iron vacancies appear at the M sites and many oxygen vacancies appear in the oxygen sublattice for valence equilibrium. Each FeO_4 complex is surrounded by seven-fold oxygen-coordinated bismuth ions. Having in mind that the mass difference of the tetragonal cations between the Fe^{3+} and M^{4+} ions, the force constants for two-particle stretching vibration between two atoms forming covalent bonds such as M-O bond, thee-particle bending vibration between atoms forming bond angles (e.g., O-M-O, Bi-O-M), and two-particle long-range forces between non-bonded atoms such as Bi-M and M-M are different in the sillenite-type bismuth ferric nanocrystals with a composition of $Bi_{12}Fe_{0.63}O_{18.945}$, as compared with the ideal sillenite-type compounds, $Bi_{12}MO_{20}$ (M = Si, Ge, Ti). Based on the features of the Raman spectra of the sillenite-type compounds of $Bi_{12}MO_{20}$ (M = Si, Ge, Ti) [12,13], the Raman band observed at 100 cm^{-1} can be assigned to the mass-dependent tetrahedral *F* mode. The strongest Raman band appearing at 125 cm^{-1} is attributed to the vibrational *E* and *F* modes of the FeO_4 unit. The combination of bending and stretching modes of Bi_3O_4 units generates the weak Raman band observed at 166 cm^{-1}, and the vibrational *F* mode of FeO_4 units results in the weak Raman band at 178 cm^{-1}. Two weak Raman bands at 300 and 305 cm^{-1} can be assigned to the vibrational *F* mode of FeO_4 units. In the frequency region between 500 and 600 cm^{-1}, a major Raman band at 567 cm^{-1} was observed, which can be ascribed to the rotation of FeO_4 units. Similarly, main Raman bands appearing near 525-550 cm^{-1} in the sillenite-structure compounds of $Bi_{12}MO_{20}$ (M = Si, Ge, Ti, Zn, and Pb) was also reported [14].

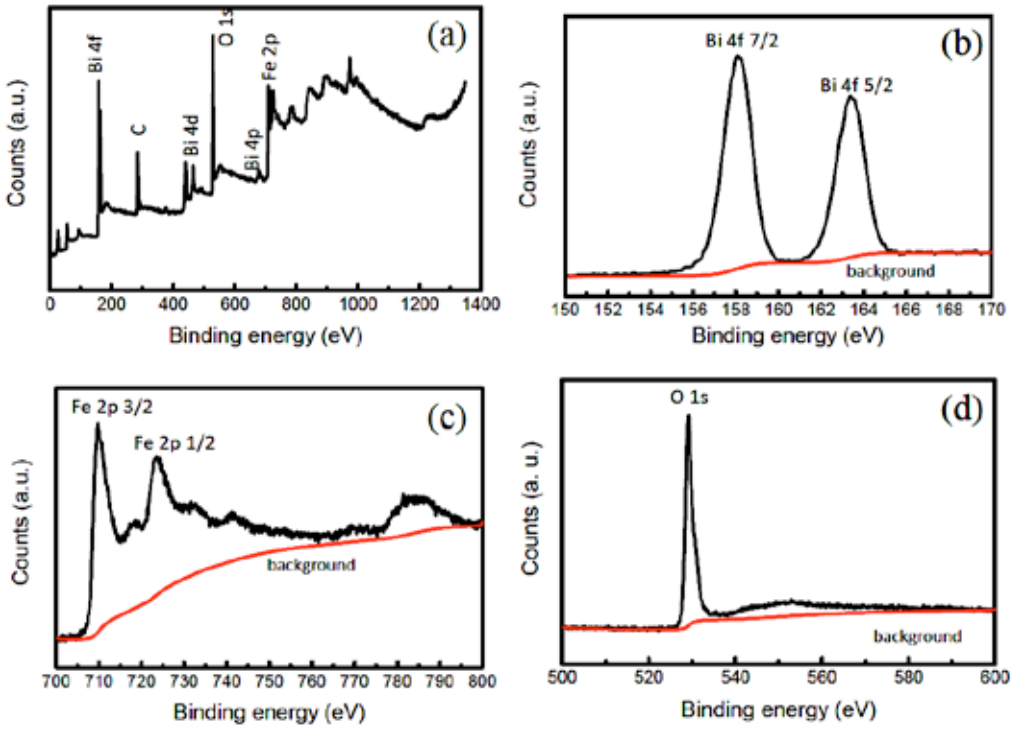

Fig.4. (a) Wide-scan XPS spectrum of the as-synthesized sillenite-type bismuth ferric nanocrystals, and (b) - (d) narrow-scan XPS spectra for Bi 4f, Fe 2p, and O 1s.

To get further insights on the valence states of the elements in the as-obtained sillenite-type bismuth ferrites, XPS measurements were performed. The wide-scan XPS spectrum of the as-produced nanocrystals is shown in Fig. 4(a), in which prominent peaks are Bi 4f, Bi 4d, and O ls peaks, and the less intense ones are identified as Bi 4p and Fe 2p peaks, indicating the existence of Bi, Fe and O elements in the sillenite-type bismuth ferric nanocrystals. The observed C element in this spectrum is probably due to the surface contamination in air. The narrow-scan XPS spectrum for Bi 4f from the sillenite-type bismuth ferric nanocrystals is shown in Fig. 4(b). Double Bi 4f XPS peaks are observed at the binding energies of 158.2 and 163.4 eV, respectively, which are the characteristics of Bi^{3+} ion [15]. The valences of Fe ions in sillenite-type bismuth ferrites are very important because the valence fluctuation of Fe ions (e.g., reduction of Fe^{3+} ions to Fe^{2+} ones) can result in high leakage current, which limits their potential applications in microelectronic devices [16]. So it is necessary to check the valences of Fe element in the sillenite-type bismuth ferric nanocrystals. Figure 4(c) shows the narrow-scan XPS spectrum of Fe 2p from the sillenite-type bismuth ferric nanocrystals, in which the Fe 2p core levels are split into $2p_{1/2}$ and $2p_{3/2}$ components due to the spin-orbit coupling, and two peaks are observed at 710.0 and 723.9 eV, corresponding to the Fe^{3+} ions [17]. No XPS peaks due to Fe^{2+} ions are observed, suggesting that Fe element in the nanocrystals exists in the valence of Fe^{3+}. The narrow XPS scan for oxygen is shown in Fig. 4(d), and just only one peak is observed at 529.2 eV, which corresponds to the O1s binding energy of O^{2-}

in the lattice [17].

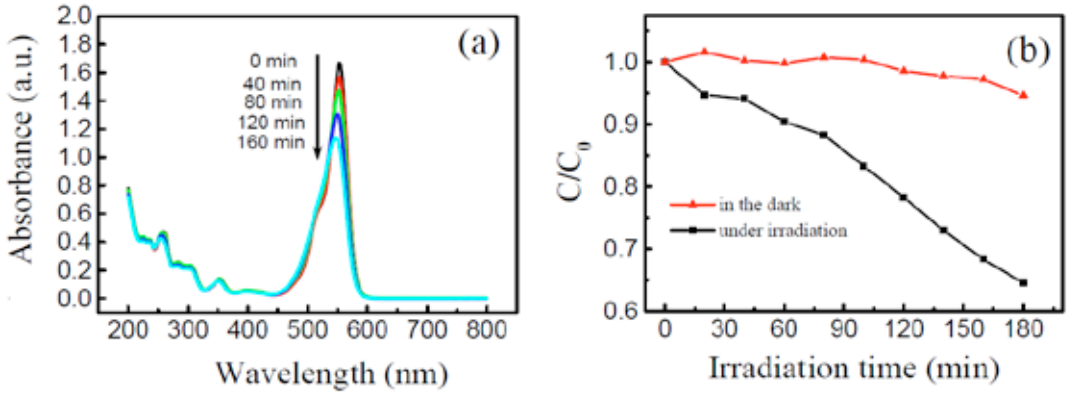

Fig.5. (a) Temporal evolution of the absorption and (b) concentration changes of the Rh B under visible-light irradiation with the presence of the sillenite-type bismuth ferric nanocrystals.

Photocatalytic activities of the as-obtained sillenite-type bismuth ferric nanocrystals were evaluated by degradation of Rh B in aqueous solution under visible-light irradiation. A representative temporal absorption spectral changes in the degradation of Rh B in the presence of the sillenite-type bismuth ferric nanocrystals under visible light irradiation, is displayed in Fig. 5(a). As shown in Fig. 5(a) the major absorption band of Rh B is near 553 nm, which is used to monitor the effect of the photocatalysis on the degradation of Rh B. Furthermore, as increasing the irradiation time the intensities of the absorption peaks at 553 nm dropped rapidly. Such apparent decrease of the absorption band at 553 nm indicates that the sillenite-type $Bi_{12}Fe_{0.63}O_{18.945}$ nanocrystals can be used as effective photocatalyst under visible-light irradiation. Figure 5(b) shows the photocatalytic activities of the as-prepared sillenite-type bismuth ferritic nanocrystals for Rh B degradation as a function of irradiation time under visible-light. The degradation rate defined as $(1\text{-}C/C_0)$, can be used to evaluate the degradation rate of the Rh B. As a typical organic contaminant, Rh B is resistant to decomposition under visible-light irradiation. For example, after 3 h visible-light irradiation without the bismuth ferritic nanocrystals, the degradation rate of Rh B was less than 5%. However, with the sillenite-type bismuth ferric nanocrystals as photocatalyst, over 35.0% of the Rh B was photolyzed after 3 h visible-light irradiation. These results demonstrate that the sillenite-type $Bi_{12}Fe_{0.63}O_{18.945}$ nanocrystals synthesized by microwave hydrothermal exhibit quite efficient photocatalytic activity under visible-light irradiation. Such an effective photocatalytic activity can be attributed to the special crystal structure of sillenite-type bismuth ferric nanocrystals. Sillenite compounds with the general formula of $Bi_{12}MO_{20\pm\delta}$ are regarded as the stabilized γ-phase Bi_2O_3 by adding M ions [4]. There exist inherent oxygen ion and cationic vacancies in the crystal structure of $Bi_{12}Fe_{0.63}O_{18.945}$. The oxygen vacancies in the semiconductor can act as trap centers of the photo-generated electrons, and thus suppress the recombination of electron hole pairs [18], which is much benefit to the photo-degradation. In addition, the incorporation of Fe ions into the crystal structure of γ-Bi_2O_3, leads to the hybrid states in the conduction band and the valence band [6], which broads the bands and favors a fair mobility of photo-generated charges, improving the photocatalytic activity. Compared with the normal TiO_2-based photocatalysts, which are only response to UV irradiation due to its large band gap (3.2 eV), the sillenite-type $Bi_{12}Fe_{0.63}O_{18.945}$ nanocrystals exhibit obvious advantage making use of the visible-light due to their

small band gap (~ 2.2 eV). To the knowledge of the authors, the photocatalytic activity of the sillenite-type $Bi_{12}Fe_{0.63}O_{18.945}$ nanocrystals synthesized by microwave-assisted hydrothermal, is for the first time reported.

4. Conclusions

Sillenite-type $Bi_{12}Fe_{0.63}O_{18.945}$ nanocrystals with hexagonal-shaped morphology and particle size range of 18 - 33 nm, were synthesized by microwave hydrothermal process, and their microstructures were examined by XRD, Raman spectra, XPS, and TEM. The XRD pattern revealed that the $Bi_{12}Fe_{0.63}O_{18.945}$ nanocrystals crystallized in the sillenite body-centered cubic *I*23 phase, and the single-crystalline nature of the sillenite-type $Bi_{12}Fe_{0.63}O_{18.945}$ nanocrystals was confirmed by HRTEM image. XPS investigations demonstrated that Fe element existed as the Fe^{3+} valence state, as well as Bi element as Bi^{3+} in the $Bi_{12}Fe_{0.63}O_{18.945}$ nanocrystals. The photocatalytic activities of the as-prepared $Bi_{12}Fe_{0.63}O_{18.945}$ nanocrystals for degradation of Rh B in aqueous solution under visible-light irradiation are clearly demonstrated, which are attributed to the small mean particle size and the unique hexagonal-shape morphology, and also the structural characteristics of the sillenite-type crystals. The present results show that the hexagonal-shaped sillenite-type bismuth ferritic nanocrystals can be used as the potential visible-light photocatalysts for degradation of organic compounds.

Acknowledgements

This work is financially supported by National Natural Science Foundation of China (Grant No. 10874065), Natural Science Foundation of Jiangsu Province (Project No. BK2007130), key projects from Ministry of Science and Technology of China (Grant Nos. 2009CB929503 and 2009ZX02101-4), the project sponsored by the Scientific Research Foundation for the Returned Overseas Chinese Scholars, State Education Ministry, and National Found for Fostering Talents of Basic Science (NFFTBS) (Project No. J0630316).

References

[1] Hoffmann MR, Martin ST, Choi W, Bahnemann DW. Environmental applications of semiconductor photocatalysis. *Chem Rev* 1995;**95:**69-96.
[2] Fox MA, Dulay MT. Heterogeneous photocatalysis. *Chem Rev* 1993;**93**:341-357.
[3] Linsebigler AL, Lu G, Yates JT. Photocatalysis on TiO_2 surfaces: principles, mechanisms, and selected results. *Chem Rev* 1995;**95**:735-758.
[4] Valant M, Suvorov D. A stoichiometric model for sillenites. *Chem Mater* 2002;**14**:3471-34767.
[5] Yao WF, Wang H, Xu XH, Zhou JT, Yang XN, Zhang Y, Shang SX, Wang M. Sillenites materials as novel photocatalysts for methyl orange decomposition. *Chem Phys Lett* 2003;**377**:501-506.
[6] Lin XP, Huang FQ, Wang WD, Xia YJ, Wang YM, Liu ML, Shi JL. Photocatalytic activity of a sillenite-type material $Bi_{25}GaO_{39}$. *Catal Comm* 2008;**9**:572-576.
[7] Zhou JK, Zou ZG, Ray AK, Zhao XS. Preparation and characterization of polycrystalline bismuth titanate $Bi_{12}TiO_{20}$ and its photocatalytic properties under visible light irradiation. *Ind Eng Chem Res* 2007;**46**:745-749.
[8] Han JT, Huang YH, Wu XJ, Wu CL, Wei W, Peng B, Huang W, Goodenough JB. Tunable synthesis of bismuth ferrites with various morphologies. *Adv Mater* 2006;**18**:2145-2148.
[9] Marquet H, Tapiero M, Merle JC, Zielinger JP, Launay JC. Determination of the factors controlling the optical background absorption in nominally undoped and doped sillenites. *Opt Mater* 1998;**11**:53-65.
[10] Egorysheva AV, Volkov VV, Burkov VI, Dudkina TD, Kargin YF. Growth and characterization of bismuth borate crystals. *Opt Mater* 1999;**13**:361-365.

[11] Rousseau DL, Bauman RP, Porto SPS. Normal mode determination in crystals. *J Raman Spectr* 1981;**10**:253-290.
[12] Venugopalan S, Ramdas AK. Raman spectra of bismuth germanium oxide and bismuth silicon oxide. *Phys Rev B* 1972;**5**:4065-4079.
[13] Leonov EI, Semenov AE, Tsherbakov AG. A combined vibrational analysis of the $Bi_{12}SiO_{20}$, $Bi_{12}GeO_{20}$, $Bi_{12}TiO_{20}$ crystals. *Fiz. Tverd. Tela* 1986;**28**:1590-1593.
[14] Burkov VI, Gorelik VS, Egorysheva AV, Kargin YF. Laser raman spectroscopy of crystals with the structure of sillenite. *J Russ Laser Res* 2001;**22**:243-267.
[15] Lee YH, Wu JM, Chen YC, Lu YH, Lin HN. Surface chemistry and nanoscale characterizations of multiferroic BiFeO3 thin films. *Electrochem Solid State Lett* 2005;**8**:F43-F46.
[16] Palkar VR, John J, Pinto R. Observation of saturated polarization and dielectric anomaly in magnetoelectric BiFeO3 thin films. *Appl Phys Lett* 2002;**80**:1628-1630.
[17] Niedrig TS, Weiss W, Schlögl R. Electronic structure of ultrathin ordered iron oxide films grown onto Pt(111). *Phys Rev B* 1995;**52**:17449-17460.
[18] He CH, Gu MY. Preparation, characterization and photocatalytic properties of $Bi_{12}SiO_{20}$ powders. *Script Mater* 2006;**55:**481-484.